www.nature.com/aps

Acta Pharmacologica Sinica

ARTICLE

Differential modulation of subthalamic projection neurons by short-term and long-term electrical stimulation in physiological and parkinsonian conditions

Cheng Xiao[1,2,3], Ya-wei Ji[1], Yi-wen Luan[1,4], Tao Jia[1], Cui Yin[1,2,3] and Chun-yi Zhou[1,2,3]

The subthalamic nucleus (STN) is one of the best targets for therapeutic deep brain stimulation (DBS) to control motor symptoms in Parkinson's disease. However, the precise circuitry underlying the effects of STN-DBS remains unclear. To understand how electrical stimulation affects STN projection neurons, we used a retrograde viral vector (AAV-retro-hSyn-eGFP) to label STN neurons projecting to the substantia nigra pars reticulata (SNr) (STN−SNr neurons) or the globus pallidus interna (GPi) (STN−GPi neurons) in mice, and performed whole-cell patch-clamp recordings from these projection neurons in ex vivo brain slices. We found that STN−SNr neurons exhibited stronger responses to depolarizing stimulation than STN−GPi neurons. In most STN−SNr and STN−GPi neurons, inhibitory synaptic inputs predominated over excitatory inputs and electrical stimulation at 20–130 Hz inhibited these neurons in the short term; its longer-term effects varied. 6-OHDA lesion of the nigrostriatal dopaminergic pathway significantly reduced inhibitory synaptic inputs in STN−GPi neurons, but did not change synaptic inputs in STN−SNr neurons; it enhanced short-term electrical-stimulation-induced inhibition in STN−SNr neurons but reversed the effect of short-term electrical stimulation on the firing rate in STN−GPi neurons from inhibitory to excitatory; in both STN−SNr and STN−GPi neurons, it increased the inhibition but attenuated the enhancement of firing rate induced by long-term electrical stimulation. Our results suggest that STN−SNr and STN−GPi neurons differ in their synaptic inputs, their responses to electrical stimulation, and their modification under parkinsonian conditions; STN−GPi neurons may play important roles in both the pathophysiology and therapeutic treatment of Parkinson's disease.

Keywords: subthalamic nucleus; electrical stimulation; substantia nigra pars reticulata; globus pallidus interna; synaptic inputs; firing; Parkinsonian mice

Acta Pharmacologica Sinica (2022) 43:1928–1939; https://doi.org/10.1038/s41401-021-00811-4

INTRODUCTION

As an important component of the basal ganglia, the subthalamic nucleus (STN) is implicated in the control of movement and action [1–5]. Abnormal neuronal activity and enhanced beta oscillations in the STN are among the critical pathophysiological features that contribute to motor symptoms in Parkinson's disease (PD) [4, 5]. Deep brain stimulation (DBS) effectively normalizes pathological beta oscillations in the STN, leading to improvements in major motor symptoms and mitigation of *L*-dopa-induced motor complications in PD, including motor fluctuations and dyskinesia [4–7]. Although several mechanisms have been postulated, the circuit bases for the therapeutic benefits of STN-DBS are far from well-understood.

Cell- and projection-specific optogenetic studies have made large strides in advancing our understanding of the circuit targets of STN-DBS. Using channelrhodopsin and halorhodopsin as actuators for bidirectional optogenetic modulation, researchers found that neither stimulation nor inhibition of STN glutamatergic neurons improved amphetamine- or apomorphine-induced rotational behavior in parkinsonian rodents, but stimulation of the hyperdirect pathway from the motor cortex to the STN did [6, 8]. Several studies have demonstrated that both excitatory and inhibitory synaptic inputs to STN neurons are modified in parkinsonian mice [9–11]. These studies stress the synaptic inputs to the STN as the key target of STN-DBS, in line with the notion that the STN-DBS with parameters that produce the most striking motor benefits likely recruits axonal fibers [4, 12]. However, because of its relatively slow opening and closing kinetics (in the order of ms), channelrhodopsin (ChR2(H134R)) may not produce STN firing rates of >100 Hz or drive glutamate release at >100 Hz. Such frequencies may require faster actuators, such as fast channelrhodopsin (ChR2(E123T/T159C)) or Chronos [7, 13, 14]. Indeed, high-frequency light stimulation of either the hyperdirect pathway via fast ChR2 or STN neurons via Chronos improves motor function in parkinsonian rodents [7, 13]. These recent optogenetic studies suggest that both synaptic inputs and STN neurons may contribute to the therapeutic benefits of STN-DBS.

The STN governs two basal ganglia output nuclei: the globus pallidus interna (GPi) and the substantia nigra pars reticulata (SNr)

[1]Jiangsu Province Key Laboratory of Anesthesiology, School of Anesthesiology, Xuzhou Medical University, Xuzhou 221004, China; [2]Jiangsu Province Key Laboratory of Anesthesia and Analgesia Application Technology, Xuzhou Medical University, Xuzhou 221004, China; [3]NMPA Key Laboratory for Research and Evaluation of Narcotic and Psychotropic Drugs, School of Anesthesiology, Xuzhou Medical University, Xuzhou 221004, China and [4]Department of Anesthesiology, Wuxi People's Hospital, Wuxi 214023, China
Correspondence: Cheng Xiao (xchengxj@xzhmu.edu.cn) or Chun-yi Zhou (chunyi.zhou@xzhmu.edu.cn)

Received: 1 September 2021 Accepted: 31 October 2021
Published online: 8 December 2021

[4, 15, 16]. STN stimulation increases glutamate levels in the SNr and GPi [17, 18], suggesting that these nuclei are recruited by STN-DBS. In addition, both electrical stimulation and chemogenetic inhibition of the SNr and GPi improve parkinsonian motor symptoms [1, 4, 5, 19–25]. Clinical studies have demonstrated that some neural networks are similarly modulated by high-frequency stimulation of the STN and GPi in PD patients [26, 27]. Together, these studies suggest that the SNr and GPi may mediate the physiological effects of STN-DBS. However, to close the gap in understanding between STN stimulation and regulation of the SNr and GPi, it is necessary to address how STN-DBS modulates the STN neurons that project to the SNr and GPi (STN−SNr and STN−GPi neurons).

In the present study, we combined AAV-assisted retrograde tracing [28] and brain slice patch-clamp recordings in STN−SNr and STN−GPi neurons. We found that STN−SNr and STN−GPi neurons were somewhat different in their intrinsic membrane properties, synaptic transmission, responses to short- and long-term electrical stimulation at 20−130 Hz, and modification in parkinsonian animals. Our results demonstrate that STN−GPi and STN−SNr neurons may be modulated differently by STN-DBS in both physiological and parkinsonian conditions.

MATERIALS AND METHODS

The care and use of animals and the experimental protocol of this study were approved by the Institutional Animal Care and Use Committee and the Office of Laboratory Animal Resources of Xuzhou Medical University under the Regulations for the Administration of Affairs Concerning Experimental Animals (1988) in China. C57BL/6 male mice were purchased from Jinan Pengyue Laboratory Animal Breeding Co. Ltd, and were group housed (≤4 per cage) on a 12 h light/dark cycle in an animal facility with stable temperature (20−22 °C) and humidity (40%–70%). Water and food were provided *ad libitum*. Efforts were made to minimize animal suffering and reduce the number of animals used.

Retrograde labeling of STN projection neurons

AAV retro-hSyn-eGFP (OBIO Technology, Shanghai, China) was microinjected into the SNr (AP, −3.10 mm; ML, 1.50 mm; DV, 4.50 mm) or the GPi (AP, − 1.30 mm; ML, 1.75 mm; DV, 4.70 mm). The mice were used for experiments after >3 weeks' recovery to allow sufficient viral expression. The location of the injection site was confirmed histologically. The sections were carefully selected to exclude the possibility that STN neurons were labeled by virus spread. For retrograde labeling of STN–SNr neurons, we selected the sections where there was a clear dark area between the labeled SNr and STN neurons. For retrograde labeling of STN–GPi neurons, we selected the sections that did not label neurons in the SNr: if the virus spread into the STN, it may retrogradely label SNr neurons. Data were included in this study only when these criteria were met.

Live brain slice preparation

The ex vivo brain slices were prepared from 12–16-wk old C57BL/6 (wild-type, WT) mice. STN neurons were recorded with patch-clamp techniques, using the protocol described previously [29–32]. In brief, the mice were deeply euthanized with CO_2, and then decapitated. The brain was removed and sectioned with a vibratome (VT-1200S, Leica) into 350 μm parasagittal slices, while immersed in ice-cold modified sucrose-based artificial cerebral spinal fluid (sACSF) containing (mM): 85 NaCl, 75 sucrose, 2.5 KCl, 1.25 NaH_2PO_4, 4.0 $MgCl_2$, 0.5 $CaCl_2$, 24 $NaHCO_3$ and 25 glucose [31, 32]. Brain slices containing the STN were allowed to recover for 1 h at 32 ± 1 °C in a holding chamber filled with sACSF, and were then transferred into normal ACSF, containing (mM): 125 NaCl, 2.5 KCl, 1.2 NaH_2PO_4, 1.2 $MgCl_2$, 2.4 $CaCl_2$, 26 $NaHCO_3$, and 11 glucose, at room temperature. One brain slice was transferred into the recording chamber and perfused (1.5–2.0 mL per min) with ACSF at 32 ± 0.5 °C. Four slices per mouse were used for recordings each day. Both sACSF and ACSF were bubbled and saturated with 95% O_2/5% CO_2 (carbogen) during experiments.

Patch-clamp recording

The neurons in brain slices were visualized with an upright microscope (FN-1, Nikon, Japan) equipped with a CCD-camera (Flash 4.0 LTE, Hamamatsu, Japan), a 4× air objective, a 40× water immersion objective (NIR APO: NA, 0.80; WD, 3.5 mm), and near-infrared and green fluorescent illumination. Whole-cell patch-clamp techniques were performed to record electrophysiological signals at a sampling rate of 10 kHz, subjected to low-pass filtering at 2 kHz with a MultiClamp 700B amplifier (Molecular Devices, CA), a Digidata 1550B analog-to-digital converter (Molecular Devices), and a pClamp 10.7 software (Molecular Devices). Patch electrodes had a resistance of 4−6 MΩ when filled with intrapipette solution (in mM): 135 K gluconate, 0.5 KCl, 5 EGTA, 0.5 $CaCl_2$, 10 HEPES, 2 Mg-ATP, and 0.1 GTP. The pH of this solution was adjusted to 7.2 with Tris-base and its osmolarity was adjusted to 300 mOsm with sucrose. The junction potential between the patch pipette and the bath solution was nulled just before gigaseal formation. Series resistance was monitored without compensation throughout the experiment. We ended the experiment if the series resistance (10 −20 MΩ) changed by >20% during whole-cell recordings and excluded any such data.

We applied a 5 mV hyperpolarizing step from a holding potential of −50 mV to STN neurons and calculated their membrane resistance according to Ohm's law. We used Clampfit 10.7 (Molecular Devices, USA) to measure the amplitude of electrical stimulation-evoked postsynaptic currents, and to count and analyze spontaneous firing. Action potentials were detected with the 'threshold search' feature in Clampfit.

A tungsten metal electrode (256 μm thick with a 3 μm tip, 0.5 MΩ) (TM33B05, WPI, Sarasota, USA) was placed 200 μm dorsoanterior to the recorded neuron and connected to a stimulus isolator (ISO-Flex, AMPI, Gaithersburg, USA) in current mode. The brain slice was stimulated by delivering a single square stimulus or a train of square stimuli (100 μs, 100 μA).

Establishment of parkinsonian mouse models

We established a hemiparkinsonian mouse model according to previous studies [31–33]. Mice were anesthetized with sodium pentobarbital (40 mg per kg) and stabilized on a stereotaxic frame (RWD life science, Shenzhen, China) for intracranial micro-injection (kdScientific, Holliston, USA). 6-OHDA (12 μg per μL, 0.5 μL) was injected in the medial forebrain bundle (MFB) (AP: + 0.5 mm, ML: 1.2 mm, DV: 4.8 mm) in the right hemisphere, while saline was injected in the left MFB. Control mice were subjected to bilateral injection of 0.5 μL saline in the MFB. To protect noradrenergic neurons from lesion, desipramine (20 mg per kg) was injected intraperitoneally 30 min before 6-OHDA injection. Two weeks later, the mice were placed in an open-field arena and their motor behavior was recorded with a video camera controlled by Ethovision XT 14 software [29, 31, 34]. After a baseline was obtained, the mice were subcutaneously injected with apomorphine (0.5 mg per kg) and, 30 min later, their rotation behavior was analyzed. A dramatic increase in the percentage of contralesional rotations represents the establishment of a hemiparkinsonian model [32, 35].

Immunohistochemistry

C57BL/6 mice were euthanized with CO_2 and subjected to cardiac perfusion with 7 mL PBS containing heparin (10 international units per mL) followed by 30 mL paraformaldehyde (PFA) (4% in PBS). The brains were then removed and post-fixed in 4% PFA for 4−6 h. After rinsing with PBS, the brains were sectioned into 30 μm

sections with a cryostat (CM1950, Leica). The sections were mounted onto microscope slides, dried at room temperature, and frozen at −20 °C.

The frozen slices were thawed at room temperature (15 min), washed twice (10 min each) with cold PBS (4 °C), permeabilized for 1 h at room temperature in PBS/0.1% Triton X-100, blocked for 45 min in PBS/10% donkey serum, incubated with primary antibodies (1:500, mouse anti-tyrosine hydroxylase (TH) IgG, Santa Cruz) in PBS/4% donkey serum at 4 °C overnight (18 h), washed three times (15 min each) in PBS, incubated with secondary antibody (1:500, Cy3-conjugated donkey anti-mouse IgG, Jackson Immunology) in PBS/4% donkey serum at room temperature for 1 h. Samples were washed three times (10 min each) in PBS, dried at room temperature, immersed in mounting medium (Vector Laboratories), and cover-slipped.

We imaged the slices with a confocal microscope (Fv-1000, Olympus, Tokyo, Japan), equipped with a 10× Plan Apo objective (numerical aperture: 0.45) and a 20× Plan Apo objective (numerical aperture: 0.75). Cy3 was excited with a 561 nm laser and detected in the range of 580−640 nm. TH-positive cells were counted with Image J [36].

Chemicals and applications

6-hydroxydopamine (6-OHDA) and ascorbic acid were purchased from Sigma Aldrich. 6-cyano-7-nitro-quinoxaline-2, 3-dione disodium salt hydrate (CNQX) and SR 95531 hydrobromide (GABAzine) were purchased from Tocris. 6-OHDA (15 μg per μL) was dissolved in 0.2% ascorbic acid, aliquoted, and stored at −20 °C. Desipramine was dissolved in saline.

Statistical analysis

To quantify the effects of electrical stimulation, the average firing frequency was obtained during the initial control period (baseline) and during electrical stimulation. The firing rate and the coefficient of variation (CV) of the firing rate during electrical stimulation were normalized to baseline. The effects of short-term and long-term electrical stimulation at 20, 50, 100, and 130 Hz were analyzed with paired *t*-tests or Wilcoxon signed rank tests depending on whether the data passed normality and equal variance tests. The effects of electrical stimulation on the firing rate and the CV of the firing rate in STN−SNr and STN−GPi neurons and between control and parkinsonian mice were compared with *t*-tests or Mann–Whitney Rank Sum tests.

In some circumstances, cumulative probability curves were plotted; the curve shifts under different conditions were analyzed with the Kolmogorov–Smirnov (K–S) test function in Clampfit.

SigmaPlot 14.0 (SPSS) was used to plot graphs and to perform statistical analyses. Values of $P < 0.05$ were considered statistically significant.

RESULTS

Membrane properties of STN–SNr and STN–GPi neurons

To address whether STN neurons projecting to the SNr and GPi (STN−SNr and STN−GPi neurons) have different membrane properties, we intracranially injected a retrograde viral vector carrying eGFP (AAV-retro-hSyn-eGFP) into either the SNr or the GPi and performed whole-cell patch-clamp recordings from eGFP-labeled STN neurons in ex vivo brain slices (Fig. 1a−c). We observed that STN−SNr and STN−GPi neurons have comparable innate excitability and firing patterns: they exhibited similar intrinsic membrane properties, including spontaneous firing rate (Figs. 1d, 1e), the CV of the spontaneous firing rate (Fig. 1f), and resting membrane potential (Fig. 1g).

To understand whether STN−SNr and STN−GPi neurons respond similarly to excitatory inputs, we injected a series of depolarizing currents into the recorded STN neurons to evoke firing. As illustrated in Fig. 1h and 1i, 20−100 pA depolarizing current induced significantly faster firing in STN−SNr neurons than in STN−GPi neurons (Fig. 1i). We also found that STN−SNr neurons had a higher membrane resistance than STN−GPi neurons (Fig. 1j).

Our data suggest that, in terms of their intrinsic membrane properties, STN−SNr neurons exhibit stronger responses to depolarizing stimulation than STN−GPi neurons.

Synaptic inputs to STN−SNr and STN−GPi neurons

In addition to a neuron's intrinsic membrane properties, the balance between excitatory and inhibitory synaptic inputs is another important factor that contributes to neuronal activity. In our experimental conditions, the reversal potentials for cations and Cl^- were 0 and −81 mV, respectively. As illustrated in Fig. 2a–e, we confirmed that electrical stimulation evoked outward (Fig. 2b, 2c) and inward (Fig. 2d, 2e) postsynaptic currents at holding potentials of 0 and −80 mV, respectively, and these evoked outward and inward currents were correspondingly blocked by GABAzine and CNQX. These results indicate that we can measure eIPSCs and eEPSCs by holding the membrane potential at 0 and −80 mV, respectively.

To address whether STN−SNr and STN−GPi neurons have different levels of excitatory and inhibitory synaptic inputs, we recorded the postsynaptic currents evoked in these neurons by electrical stimulation (100 μs, 100 μA) (Fig. 2f). In line with our previous study [30], stimulation evoked a compound postsynaptic current (ePSC) in STN neurons held at −50 mV (Fig. 2g, 2i). At −50 mV, inhibitory postsynaptic currents were outward (upward) currents, whereas excitatory postsynaptic currents were inward (downward) currents [30]. Thus, the direction of the ePSC is determined by the predominance of excitatory or inhibitory synaptic inputs. We observed either outward (type 1 neuron, Fig. 2g) or inward (type 2 neuron, Fig. 2i) ePSCs in STN neurons (held at −50 mV).

Low- (20 Hz) or high- (100−130 Hz) frequency stimulation respectively exacerbates or improves motor deficits in parkinsonian animals and PD patients [4–6], suggesting that electrical stimulation at low and high frequencies exerts different effects on the motor-related neural circuits. We therefore examined modulation of neuronal firing in the STN by 20−130 Hz electrical stimulation. In type 1 neurons, 1 s electrical stimulation at 20, 50, 100, and 130 Hz inhibited neuronal firing (Fig. 2h) but in type 2 neurons, electrical stimulation increased neuronal firing (Fig. 2j). Most STN−SNr and STN−GPi neurons were type 1 neurons (Fig. 2k). The outward currents in type 1 STN−GPi neurons were significantly greater than those in type 1 STN−SNr neurons (Fig. 2l). The amplitude of inward currents was similar in type 2 STN−SNr and STN−GPi neurons (Fig. 2l). In type 1 neurons, electrical stimulation at ≥50 Hz inhibited firing to a much greater extent than stimulation at 20 Hz (Fig. 2m). STN−SNr and STN−GPi neurons were similarly inhibited by electrical stimulation at 20−130 Hz (Fig. 2m). In type 2 STN−SNr neurons, 50 Hz electrical stimulation increased the firing rate more robustly than stimulation at other frequencies (Fig. 2n). In type 2 STN−GPi neurons, electrical stimulation increased the firing rate similarly for all frequencies (20–130 Hz) (Fig. 2n). 50 Hz electrical stimulation increased the firing rate to a greater degree in STN−SNr neurons than STN−GPi neurons (Fig. 2n).

As illustrated in Fig. 2o, STN−GPi neurons exhibited larger eIPSCs (at 0 mV) than STN−SNr neurons but similar eEPSCs (at −80 mV). We applied paired electrical pulses separated by 50 ms to brain slices to evoke paired eIPSCs and eEPSCs (Fig. 2p). STN−GPi neurons displayed smaller paired-pulse ratios (PPRs) for eIPSCs than STN−SNr neurons, but PPRs for eEPSCs were similar in STN–GPi and STN−SNr neurons (Fig. 2q). These results suggest that presynaptic GABAergic terminals form stronger synaptic connections with STN−GPi neurons than STN−SNr neurons and that these terminals have a higher release probability.

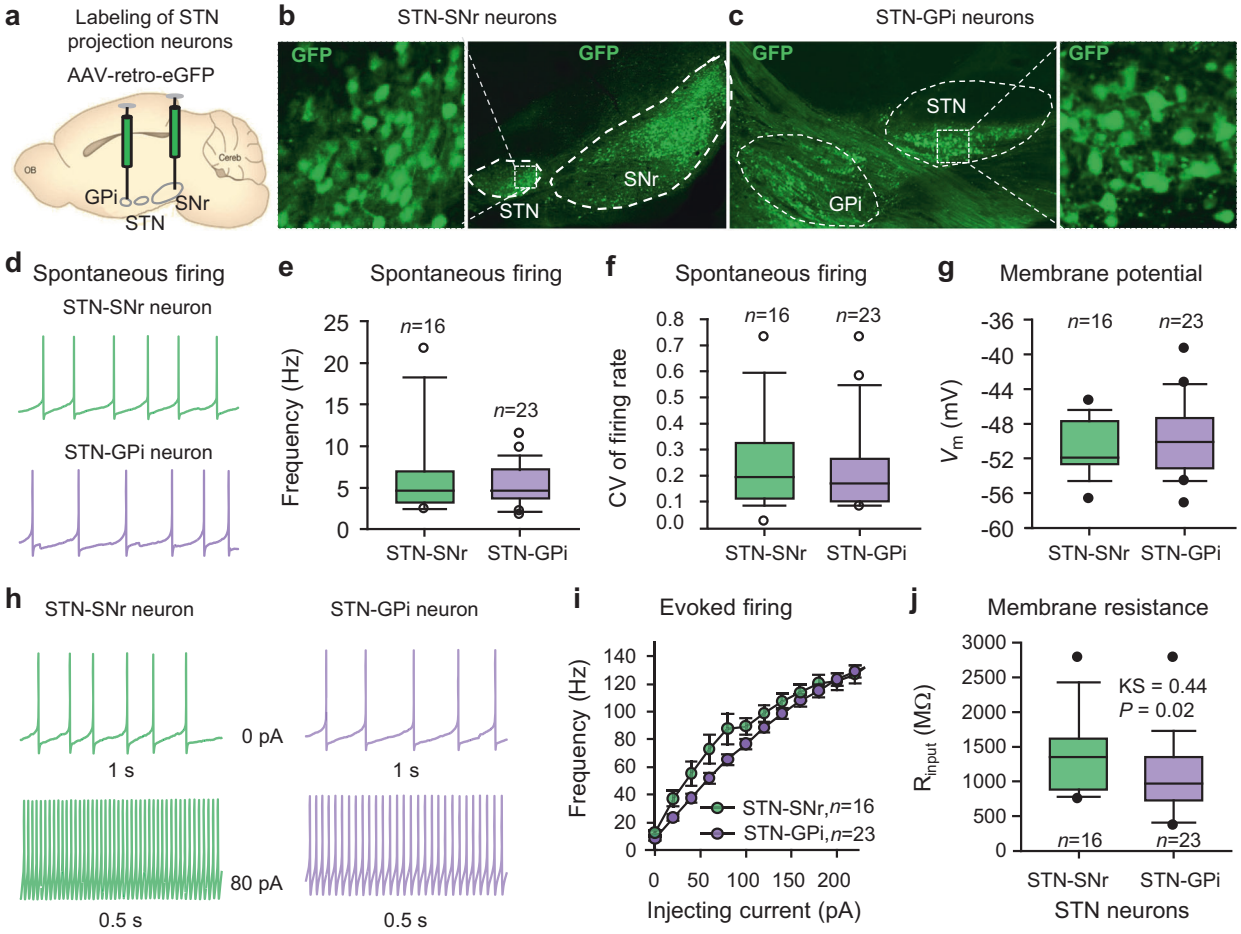

Fig. 1 Intrinsic membrane properties of STN−SNr and STN−GPi neurons. a AAV-retro-hSyn-eGFP was intracranially injected into the SNr or the GPi in mice ($n = 4$ each) to label SNr- or GPi-projecting STN neurons (STN−SNr or STN−GPi neurons). After 2−3 weeks, the mice were sacrificed for imaging of eGFP-labeled STN neurons. **b–c** Typical image showing retrogradely labeled STN−SNr neurons (**b**) and STN−GPi neurons (**c**). **d** 1 s trace of spontaneous firing in an STN−SNr neuron (upper panel) and an STN−GPi neuron (lower panel). **e** Boxplot showing the spontaneous firing rate in STN−SNr and STN−GPi neurons ($T = 323$, $P = 0.94$, Mann–Whitney Rank Sum Test). **f** Boxplot showing the CV of firing rate in STN−SNr and STN−GPi neurons ($T = 394$, $P = 0.35$, Mann–Whitney Rank Sum Test). **g** Boxplot showing the resting membrane potential (V_m) in STN−SNr and STN−GPi neurons ($t = 0.88$, $P = 0.39$, two-tailed t-test). **h** Typical traces showing spontaneous firing (upper panels) and depolarizing current-injection-evoked firing (lower panels) in an STN−SNr neuron (left panels) and an STN−GPi neuron (right panels). **i** Summary of firing frequency upon current injection in STN−SNr (green circles) and STN−GPi (purple circles) neurons (Group, $F = 5.83$, $P = 0.02$; Current, $F = 364.73$, $P < 0.001$; Group×Current, $F = 1.74$, $P = 0.13$; two-way repeated measures ANOVA). **j** Summary of the membrane resistance (R_{input}) in STN−SNr and STN−GPi neurons (KS = 0.44, $P = 0.02$, K–S test).

We next analyzed the correlations between electrical-stimulation-induced changes in the firing rate and the amplitudes of ePSCs (at −50 mV), eIPSCs (at 0 mV), and eEPSCs (at −80 mV) (Fig. 2r). We normalized the firing rate during electrical stimulation at 20, 50, 100, and 130 Hz to the firing rate during baseline. Our data show that the normalized firing rate has a better correlation with the ePSC amplitude than with the eIPSC or eEPSC amplitude. Therefore, the direction and amplitude of the ePSC is a better predictor of the effects of electrical stimulation on neuronal firing than the eIPSCs or eEPSCs.

Responses in STN−SNr and STN−GPi neurons to longer-duration electrical stimulation

In clinical settings, persistent stimulation is required to maintain the therapeutic benefits of DBS [1, 4, 5, 37, 38]. Furthermore, upon repetitive stimulation, the strength of excitatory and inhibitory synaptic transmission can be altered in different ways [39]. Therefore, it is necessary to explore neuronal responses to stimulation of longer duration. Because they account for >70% of recorded neurons, we examined the firing responses of type 1 STN neurons (neurons with an outward ePSC at −50 mV) to longer pulse trains.

From the time courses of instantaneous firing rates in STN neurons during longer electrical stimulation (30 s), we observed two response phases (Fig. 3). The first phase was an initial decrease (Fig. 3a, 3g) or increase (Fig. 3d, 3j) in the firing rate that occurred within a few seconds of the onset of electrical stimulation and showed little variability. The second phase was a reduction (Fig. 3a, 3g) or increase (Fig. 3d, 3j) in the firing rate accompanied by increased firing variability; this phase appeared several seconds after the onset of electrical stimulation. The variability stabilized around 10–30 s after the initiation of the electrical stimulation.

Although 20–130 Hz electrical stimulation partially or completely inhibited most type 1 STN neurons in the first few seconds, consistent with the results for 1 s stimulation described in the section above, the longer-term effects varied (Fig. 3a−k). The overall effect of 30 s 20 Hz electrical stimulation was inhibitory in some neurons

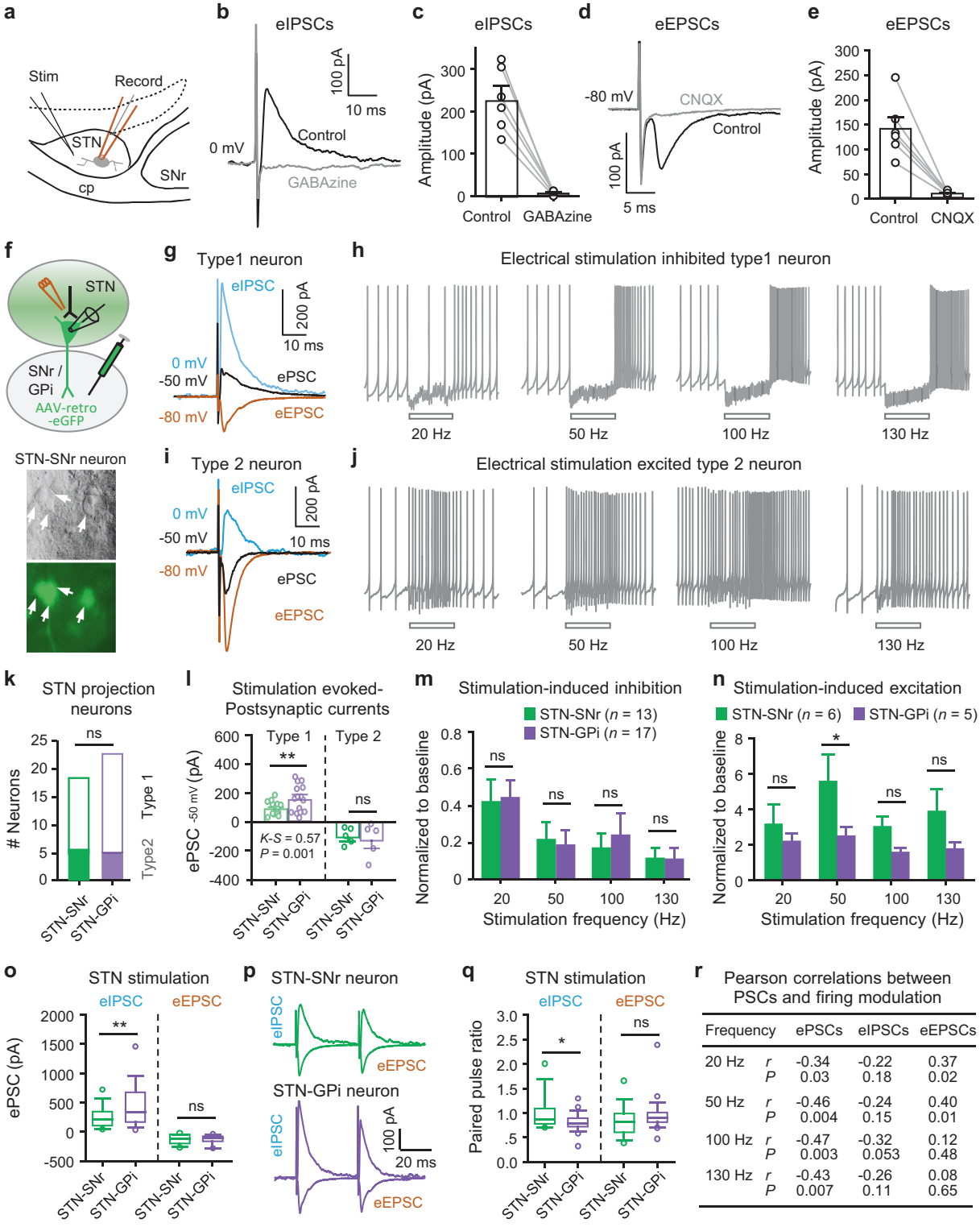

Frequency		ePSCs	eIPSCs	eEPSCs
20 Hz	r	-0.34	-0.22	0.37
	P	0.03	0.18	0.02
50 Hz	r	-0.46	-0.24	0.40
	P	0.004	0.15	0.01
100 Hz	r	-0.47	-0.32	0.12
	P	0.003	0.053	0.48
130 Hz	r	-0.43	-0.26	0.08
	P	0.007	0.11	0.65

(Fig. 3a–c) but excitatory in others (Fig. 3d–f). A similar phenomenon was observed for 130 Hz electrical stimulation (inhibitory: Fig. 3g–l; excitatory: Fig. 3j–l). Given that 1 s stimulation consistently produced only inhibition in type 1 STN neurons (Fig. 2h), these results suggest that long-term (30 s) and short-term (1 s) electrical stimulation differ in how they modulate firing in STN neurons. Quantitative analysis showed that (1) in comparison with short-term electrical stimulation, long-term electrical stimulation induced weaker inhibition (Fig. 3m, 3o); (2) long-term electrical stimulation significantly increased the CV of the firing rate in both STN–SNr (Fig. 3n) and STN–GPi neurons (Fig. 3p). These data suggest that, in type 1 STN neurons, the inhibitory effect of electrical stimulation varies with time and long-term stimulation tends to exacerbate the irregularity of the firing pattern.

Fig. 2 Electrical-stimulation-evoked responses in STN−SNr and STN−GPi neurons. a The whole-cell patch-clamp technique was used to record electrical-stimulation-evoked postsynaptic currents in STN neurons in mice. **b** Electrical stimulation (100 μs, 100 μA) evoked an outward current (black trace) (evoked inhibitory postsynaptic current, eIPSC) in a voltage-clamped STN neuron ($V_H = 0$ mV), which was blocked by 10 μM GABAzine, a $GABA_A$ receptor blocker (gray trace). **c** The amplitude of eIPSCs in STN neurons in the absence (Control) and presence (GABAzine) of GABAzine. $t = 5.56$, $P = 0.003$, $n = 6$, Control vs GABAzine, two-tailed paired *t*-test. **d** Electrical stimulation (100 μs, 100 μA) evoked an inward current (black trace) (evoked excitatory postsynaptic current, eEPSC) in a voltage-clamped STN neuron ($V_H = -80$ mV), which was blocked by 20 μM CNQX, a glutamate receptor blocker (gray trace). **e** The amplitude of eEPSCs in STN neurons in the absence (Control) and presence (CNQX) of CNQX. $t = 7.35$, $P = 0.0007$, $n = 6$, Control vs CNQX, two-tailed paired *t*-test. **f** AAV-retro-hSyn-eGFP was used to label STN−SNr and STN−GPi neurons (four mice in each group), and the whole-cell patch-clamp technique was performed to record eGFP-labeled STN neurons. **g** Postsynaptic currents were recorded upon electrical stimulation from a voltage-clamped type 1 STN neuron held at 0 (cyan), −50 (black), and −80 (brown) mV. The postsynaptic currents are respectively eIPSCs, ePSCs, and eEPSCs. **h** 20, 50, 100, and 130 Hz electrical stimulation (1 s) inhibited firing in a current-clamped type 1 neuron. **i** eIPSCs, ePSCs, and eEPSCs were recorded upon electrical stimulation from a voltage-clamped type 2 STN neuron. **j** 20, 50, 100, and 130 Hz electrical stimulation (1 s) enhanced firing in a current-clamped type 2 neuron. **k** The number of type 1 and type 2 STN–SNr and STN–GPi neurons ($x^2 = 0.13$, $P = 0.71$, Chi-square test). **l** Summary of the amplitude of ePSCs in type 1 STN−SNr neurons (dark green, $n = 13$), type 1 STN−GPi neurons (purple, $n = 17$), type 2 STN−SNr neurons (dark green, $n = 5$), and type 2 STN−GPi neurons (purple, $n = 5$). Type 1: $K\text{-}S = 0.57$, $P = 0.001$, STN−SNr vs STN−GPi, K–S test. Type 2: $t = 0.54$, $P = 0.61$, STN−SNr vs STN−GPi, two-tailed *t*-test. **m** Firing rates in type 1 STN neurons during 1 s electrical stimulation at 20, 50, 100, and 130 Hz were normalized to the firing rates during baseline. 20 Hz: $t = 0.10$, $P = 0.92$; 50 Hz: $t = 0.21$, $P = 0.93$; 100 Hz: $t = 0.74$, $P = 0.47$; 130 Hz: $t = 0.07$, $P = 0.95$; STN−SNr vs STN−GPi, two-tailed *t*-test. **n** Firing rates in type 2 STN neurons during 1 s electrical stimulation at 20, 50, 100, and 130 Hz were normalized to firing rates during baseline. 20 Hz: $t = 1.34$, $P = 0.24$; 50 Hz: $t = 2.51$, $P = 0.03$; 100 Hz: $t = 2.15$, $P = 0.07$; 130 Hz: $t = 0.93$, $P = 0.38$; STN−SNr vs STN−GPi, two-tailed *t*-test. **o** Summary of the amplitude of eIPSCs and eEPSCs in STN−SNr neurons (dark green, $n = 18$) and STN−GPi neurons (purple, $n = 22$). eIPSCs: $t = 8.28$, $P < 0.0001$; eEPSCs: $t = 0.05$, $P = 0.96$; STN−SNr vs STN−GPi, two-tailed *t*-test. **p** Typical traces of eIPSCs and eEPSCs in an STN−SNr neuron and an STN−GPi neuron. **q** Summary of paired-pulse ratios of eIPSCs and eEPSCs in STN−SNr neurons (dark green, $n = 18$) and STN−GPi neurons (purple, $n = 22$). eIPSCs: $t = 2.26$, $P = 0.03$; eEPSCs: $t = 0.36$, $P = 0.72$; STN−SNr vs STN−GPi, two-tailed *t*-test. **r** Spearman rank correlations between the normalized firing rates during 1 s electrical stimulation and the amplitudes of ePSCs, eIPSCs, and eEPSCs in STN neurons ($n = 27$).

6-OHDA lesion alters synaptic transmission in STN−SNr and STN−GPi neurons

To address whether synaptic transmission is altered in STN−SNr and STN−GPi neurons in parkinsonian mice, we injected 6-OHDA intracranially in the MFB in the right hemisphere to establish a hemiparkinsonian mouse model (Fig. 4a–d) and then performed whole-cell patch-clamp recordings in STN−SNr and STN−GPi neurons in brain slices from the right hemisphere (Fig. 4e). We observed that unilateral 6-OHDA injection in the MFB lesioned most of the dopaminergic neurons in the ipsilesional substantia nigra pars compacta (SNc) (Figs. 4b, 4c) and impaired locomotion in mice (Fig. 4d). These data indicate that the hemiparkinsonian mouse model was successfully established. We then recorded eIPSCs and eEPSCs in STN neurons by holding membrane potentials at 0 mV and −80 mV, respectively (Fig. 4f, 4h). We found no difference between control and parkinsonian mice in either the amplitude of the first eIPSC or the first eEPSC evoked by paired electrical stimulation or in the paired-pulse ratio of eIPSCs or eEPSCs in STN−SNr neurons in the ipsilesional side (Fig. 4f, 4g). Interestingly, in STN–GPi neurons, 6-OHDA lesion reduced the amplitude of the first eIPSC and increased the PPR of eIPSCs, without altering the amplitude or PPR of eEPSCs (Fig. 4h, 4i). The selective impairment to inhibitory synaptic inputs in STN−GPi neurons in parkinsonian mice reversed the balance of excitation and inhibition in STN−GPi neurons, but not in STN–SNr neurons, resulting in an increased proportion of type 2 STN−GPi neurons in parkinsonian mice (Fig. 4j). The ePSCs in type 1 and type 2 STN−SNr neurons did not differ between control and parkinsonian mice (Figs. 4k, 4l); by contrast, ePSCs in type 1 but not type 2 STN−GPi neurons were significantly reduced in parkinsonian mice (Fig. 4m, 4n). Therefore, in parkinsonian mice, the balance between excitatory and inhibitory synaptic inputs in STN−GPi neurons is disrupted, favoring excitation, whereas the balance remains normal in STN−SNr neurons.

6-OHDA lesion alters responses to electrical stimulation in STN−SNr and STN−GPi neurons

We next tested whether the firing rate and the CV of the firing rate in STN−SNr and STN−GPi neurons are regulated by short-term and long-term electrical stimulation at 20−130 Hz differently in control and parkinsonian mice. To fulfill this goal, we normalized the firing rate and the CV of the firing rate during electrical stimulation to that during baseline and plotted cumulative probability curves of the normalized values in control and parkinsonian mice (Fig. 5, Fig. 6). Significant leftward or rightward shift in the curve in parkinsonian mice relative to control mice represents a decrease or an increase in the parameter on the *x*-axis.

Our data show that both short-term and long-term electrical stimulation at 20−130 Hz inhibited type 1 STN−SNr neurons more strongly in parkinsonian mice than in control mice (Fig. 5a–h). Long-term electrical stimulation at 20−130 Hz exerted similar effects on the CV of the firing rate in STN−SNr neurons in parkinsonian mice and control mice (Fig. 5i–l). For STN−GPi neurons, we found that the short-term electrical-stimulation-induced increase in the firing rate was much stronger in parkinsonian mice than in control mice (Fig. 6a−d); by contrast, long-term electrical stimulation reduced the firing rate (values <1 on the *x*-axis) much more in parkinsonian mice than in control mice, but increased the firing rate (values >1 on the *x*-axis) much less (Fig. 6e−h); long-term electrical stimulation at 20 and 50 Hz significantly increased the CV of the firing rate in parkinsonian mice compared with control mice, but long-term electrical stimulation at 100 and 130 Hz increased the CV of the firing rate similarly in parkinsonian mice and control mice (Fig. 6i−l).

These data suggest that 6-OHDA lesion modifies the excitatory–inhibitory balance in STN−GPi neurons, enhances the inhibition of STN−SNr and STN−GPi neurons induced by long-term electrical stimulation, and exacerbates the firing irregularities induced in STN−GPi neurons by long-term, low-frequency electrical stimulation.

DISCUSSION

Although synaptic inputs play a minor role in maintaining spontaneous firing in STN neurons [40, 41], they are critical in shaping the firing rate and firing pattern [42, 43]. Moreover, synaptic inputs to STN neurons, especially the hyperdirect pathway, are targets of DBS to relieve parkinsonian motor symptoms [4, 6, 7, 12, 19, 44]. It is still unknown whether STN neurons projecting to different downstream pathways exhibit similar responses to DBS. In the classical standpoint, the STN

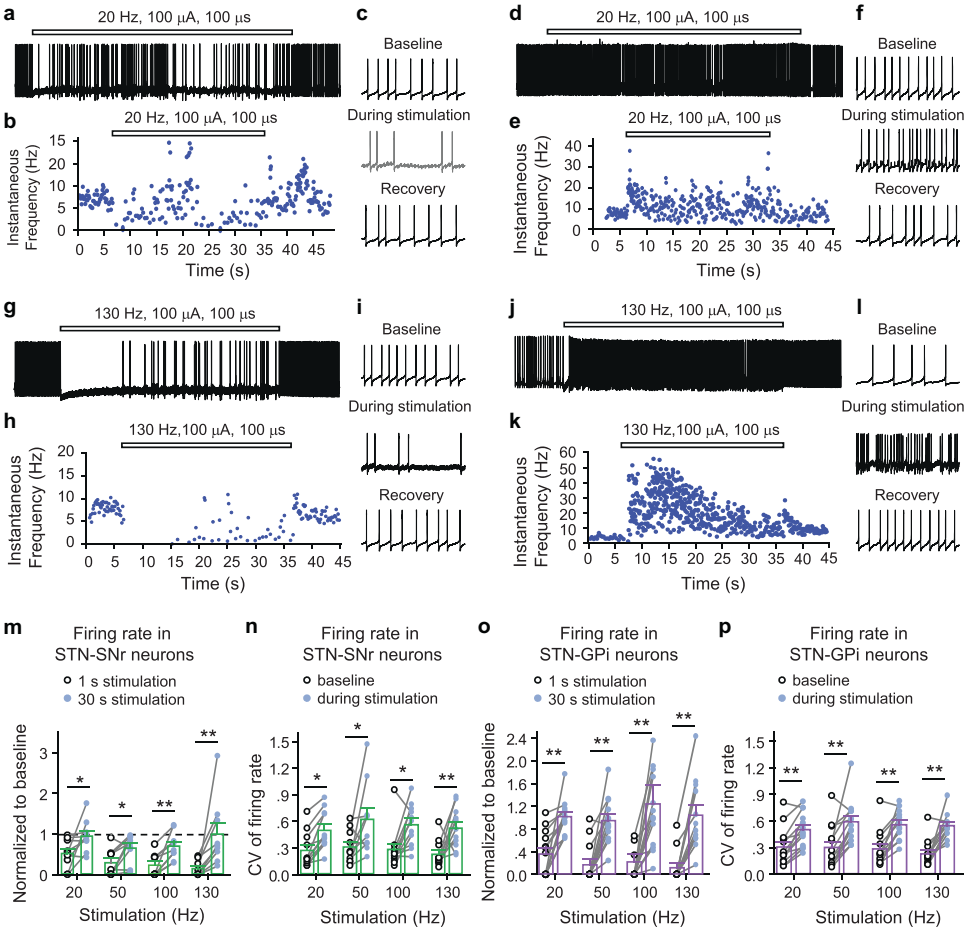

Fig. 3 Effects of long-term stimulation on STN−SNr and STN−GPi neurons. a–c 30 s 20 Hz electrical stimulation partially inhibited firing in a type 1 STN−SNr neuron (**a**, typical trace; **b**, time course; **c**, 1 s trace under different conditions). **d–f** 30 s 20 Hz electrical stimulation enhanced firing in a type 1 STN−SNr neuron (**d**, typical trace; **e**, time course; **f**, 1 s trace under different conditions). **g–i** 30 s 130 Hz electrical stimulation partially inhibited firing in a type 1 STN−SNr neuron (**g**, typical trace; **h**, time course; **i**, 1 s trace under different conditions). **j–l** 30 s 130 Hz electrical stimulation enhanced firing in a type 1 STN−SNr neuron (**j**, typical trace; **k**, time course; **l**, 1 s trace under different conditions). **m** Firing rates in type 1 STN−SNr neurons during 1 s and 30 s electrical stimulation at 20, 50, 100, and 130 Hz were normalized to baseline. 20 Hz: $t = 2.25$, $P = 0.04$, 1 s vs 30 s, two-tailed paired *t*-test; 50 Hz: $t = 2.86$, $P = 0.02$, 1 s vs 30 s, two-tailed paired *t*-test; 100 Hz: Z-Statistic = 2.67, $P = 0.004$, 1 s vs 30 s, two-tailed Wilcoxon Signed Rank test; 130 Hz: Z-statistic = 2.67, $P = 0.004$, 1 s vs 30 s, two-tailed Wilcoxon Signed Rank test. $n = 9$. **n** 30 s electrical stimulation increased the CV of the firing rate in type 1 STN−SNr neurons. 20 Hz: $t = 2.56$, $P = 0.02$; 50 Hz: $t = 2.24$, $P = 0.04$; 100 Hz: $t = 2.82$, $P = 0.01$; 130 Hz: $t = 3.62$, $P = 0.002$; 30 s stimulation vs baseline, two-tailed paired *t*-test. $n = 9$. **o** Firing rates in type 1 STN−GPi neurons during 1 s and 30 s electrical stimulation at 20, 50, 100, and 130 Hz were normalized to baseline. 20 Hz: $t = 5.08$, $P = 0.0003$; 50 Hz: $t = 5.78$, $P < 0.0001$; 100 Hz: $t = 3.22$, $P = 0.008$; 130 Hz: $t = 6.38$, $P < 0.0001$, 1 s vs 30 s, two-tailed paired *t*-test. $n = 13$. **p** 30 s electrical stimulation increased the CV of the firing rate in type 1 STN−GPi neurons. 20 Hz: $t = 2.48$, $P = 0.02$; 50 Hz: $t = 3.03$, $P = 0.006$; 100 Hz: $t = 3.52$, $P = 0.002$; 130 Hz: $t = 5.25$, $P < 0.0001$; 30 s stimulation vs baseline, two-tailed paired *t*-test. $n = 11$.

regulates the thalamocortical pathway and movement via the SNr and GPi [1, 4, 19]: thus, we attempted to elaborate the mechanisms by which electrical stimulation modulates STN−SNr and STN−GPi neurons. We found that STN−SNr and STN−GPi neurons differed in their intrinsic membrane properties, synaptic transmission, and responses to short- and long-term electrical stimulation at 20−130 Hz. Above all, the inhibitory synaptic inputs in STN−GPi neurons were selectively impaired in parkinsonian mice, resulting in distinct responses to short-term and long-term electrical stimulation in STN−GPi neurons. Our results suggest that STN−GPi neurons are significantly modified in the parkinsonian condition, but may be restored by STN-DBS.

Intrinsic membrane properties and synaptic inputs are two major factors governing and shaping neuronal excitability. We observed that STN−SNr and STN−GPi neurons had several similar intrinsic parameters, such as resting membrane potential, firing rate, and firing pattern; by contrast, STN−SNr neurons exhibited higher resting membrane resistance and stronger responses to depolarizing stimulation. We used ePSCs to represent the predominance of excitatory and inhibitory synaptic inputs and demonstrated that ePSCs were better than eIPSCs and eEPSCs in predicting inhibition (type 1) and excitation (type 2) of STN neurons by short-term electrical stimulation. We found that type 1 neurons accounted for most of the STN−SNr and STN−GPi neurons, consistent with previous morphological studies showing that GABAergic terminals comprise ~60% of the total boutons on STN neurons [15, 45, 46], and consistent with a clinical electrophysiological study showing that short-term DBS inhibits most STN neurons [47]. Our data reveal that type 1 STN−GPi neurons exhibit greater eIPSCs than type 1 STN−SNr neurons. Therefore, the effect of electrical stimulation on STN neurons depends on both intrinsic membrane properties and on the predominance of excitatory or inhibitory synaptic inputs.

In the present study, we found a dramatic difference in the modulation of type 1 STN−SNr and STN−GPi neurons by short-

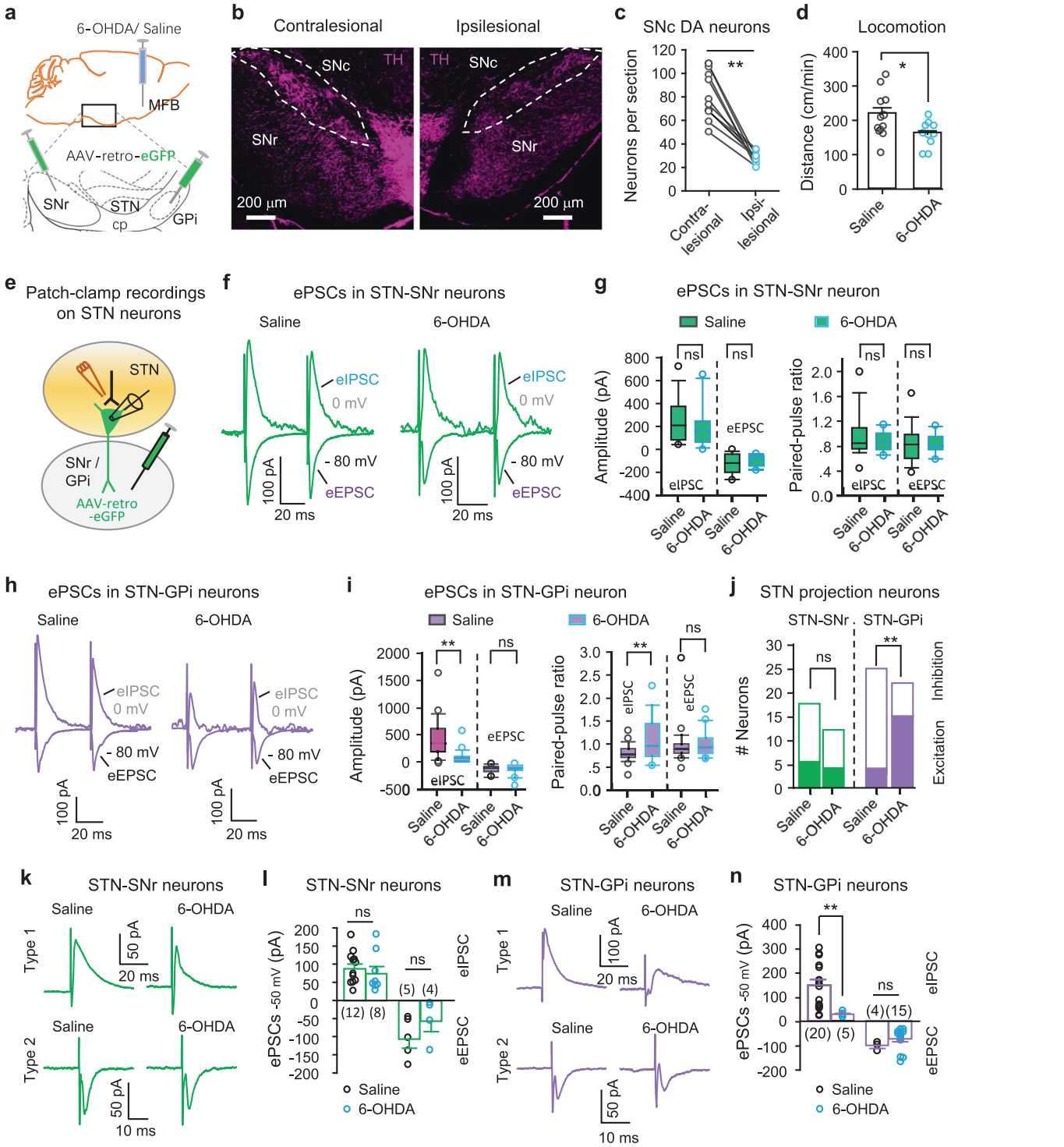

term and long-term electrical stimulation. Although short-term electrical stimulation consistently inhibited STN neurons, long-term electrical stimulation caused either diminished inhibition or even excitation. We postulate that long-term electrical stimulation may attenuate inhibitory drive by activating presynaptic $GABA_B$ autoreceptors [48, 49], reducing Cl^- gradients between the extracellular medium and the cytoplasm [43], and even activating cation channels [41, 43]. Steiner et al. demonstrated that during 1 s repetitive stimulation of the STN, eEPSCs decay more robustly than eIPSCs [39], which seems inconsistent with our results and the results from other studies [41, 43, 48, 49]. It is noteworthy that, unlike the present study, Steiner et al. isolated eIPSCs and eEPSCs pharmacologically [39]. We cannot rule out the possibility that blocking either glutamate receptors or $GABA_A$ receptors may change the circuit outcomes of electrical stimulation. Nevertheless, our results argue that one should be cautious in explaining the biophysical bases of DBS using the results obtained from short-term electrical stimulation and hint that uniform inhibition or stimulation of neuronal activity may not replicate the effects of long-term electrical stimulation in the STN.

Fig. 4 Synaptic inputs in STN−SNr and STN−GPi neurons are differentially modified in parkinsonian mice. a AAV-retro-hSyn-eGFP was injected in the SNr or GPi to label STN−SNr or STN−GPi neurons. 6-OHDA was injected in the medial forebrain bundle (MFB) in the right hemisphere to establish a hemiparkinsonian mouse model. **b** Dopaminergic (DA) neurons were labeled with tyrosine hydroxylase (TH)-antibody (purple) in a brain section from a mouse subjected to 6-OHDA lesion in the right hemisphere. **c** Summary of DA neurons in each section. $t = 9.17$, $P < 0.0001$, $n = 9$, ipsilesional vs contralesional, two-tailed t-test. **d** Distance traveled within 20 min in an open-field arena was reduced in 6-OHDA mice. $t = 4.88$, $P < 0.0001$, Saline ($n = 12$) vs 6-OHDA ($n = 10$), two-tailed t-test. **e** Diagram of the patch-clamp recordings in STN−SNr or STN−GPi neurons. **f** Paired electrical-stimulation-evoked eIPSCs (at 0 mV) and eEPSCs (at −80 mV) in an STN−SNr neuron in a Saline mouse (left panel) and in a different STN−SNr neuron in a 6-OHDA mouse (right panel). **g** The amplitude (left panel) of eIPSCs (>0 pA) ($t = 0.43$, $P = 0.67$, Saline vs 6-OHDA, two-tailed t-test) and eEPSCs (<0 pA) ($t = 1.08$, $P = 0.29$, Saline vs 6-OHDA, two-tailed t-test) and the paired- pulse ratio (right panel) of eIPSCs ($t = 0.78$, $P = 0.46$, Saline vs 6-OHDA, two-tailed t-test) and eEPSCs ($t = 0.10$, $P = 0.92$, Saline vs 6-OHDA, two-tailed t-test) in STN−SNr neurons (Saline, $n = 18$; 6-OHDA, $n = 12$) in Saline ($n = 4$) and 6-OHDA ($n = 3$) mice. **h** Paired electrical-stimulation-evoked eIPSCs and eEPSCs in an STN−GPi neuron in a Saline mouse (left panel) and in a different STN−GPi neuron in a 6-OHDA mouse (right panel). **i** The amplitude (left panel) of eIPSCs ($t = 4.19$, $P = 0.0001$, Saline vs 6-OHDA, two-tailed t-test) and eEPSCs ($t = 0.09$, $P = 0.92$, 6-OHDA vs Saline, two-tailed t-test), and the paired-pulse ratio (right panel) of eIPSCs ($t = 2.71$, $P = 0.01$, Saline vs 6-OHDA, two-tailed t-test) and eEPSCs ($t = 0.13$, $P = 0.90$, Saline vs 6-OHDA, two-tailed t-test) in STN−GPi neurons (Saline, $n = 25$; 6-OHDA, $n = 22$) in Saline ($n = 4$) and 6-OHDA ($n = 4$) mice. **j** Proportions of type 1 and type 2 STN−SNr and STN−GPi neurons in Saline and 6-OHDA mice. STN−SNr: $x^2 = 0.16$, $P = 0.68$; STN−GPi: $x^2 = 15.13$, $P = 0.0001$; Saline vs 6-OHDA, Chi-Square test. **k** ePSCs in type 1 (upper panels) and type 2 (lower panels) in STN−SNr neurons in Saline (left panels) and 6-OHDA mice (right panels). **l** The amplitudes of ePSCs in type 1 and type 2 STN−SNr neurons in Saline ($n = 4$) and parkinsonian ($n = 3$) mice. Type 1: $t = 0.59$, $P = 0.56$; Type 2: $t = 1.28$, $P = 0.24$; Saline vs 6-OHDA, two-tailed t-test. Numbers in brackets indicate numbers of recorded neurons. **m** ePSCs in type 1 (upper panels) and type 2 (lower panels) STN−GPi neurons in Saline (left panels) and 6-OHDA mice (right panels). **n** The amplitudes of ePSCs in type 1 and type 2 STN−GPi neurons in Saline ($n = 4$) and parkinsonian ($n = 4$) mice. Type 1: $t = 5.05$, $P = 0.0001$; Type 2: $P = 1.74$, $P = 0.12$; Saline vs 6-OHDA, two-tailed t-test. Numbers in brackets indicate numbers of recorded neurons.

Hyperactivity in STN neurons is commonly reported in parkinsonian animals [31, 32]. Some elegant cell-specific and projection-specific optogenetic studies have demonstrated that cortical glutamatergic inputs and pallidal GABAergic inputs are reduced/enhanced in parkinsonian rodents, respectively [9–11]. These results seem contradictory to the reported hyperactivity in STN neurons, and suggest that the alterations in cortical and pallidal inputs may be compensatory mechanisms to prevent STN neurons from over-excitation [9–11]. In the present study, we observed that lesion of SNc dopaminergic neurons differentially altered the synaptic inputs to STN−SNr and STN−GPi neurons: it did not change eEPSCs and eIPSCs in STN−SNr neurons but it impaired eIPSCs without altering eEPSCs in STN−GPi neurons. Consistent with these modifications, in parkinsonian mice, the proportion of type 2 STN−GPi neurons increased significantly, but that of type 2 STN−SNr neurons did not change, and short-term electrical stimulation increased the firing rate in more STN−GPi neurons than STN−SNr neurons. Discrepancies between our data and previous optogenetic studies may be associated with the differences between optogenetic and electrical stimulation. Optogenetic stimulation cell-specifically activates particular types of synaptic terminals in the illuminated region. By contrast, electrical stimulation recruits many types of synaptic terminals in a much smaller region around the stimulating electrode, and causes the release of multiple neurotransmitters, such as GABA, glutamate, dopamine, and histamine, etc. GABAergic and glutamatergic terminals tend to be regulated by other neurotransmitters [32, 50–52]. Thus, optogenetic studies are valuable for dissecting neural circuits, but electrical stimulation is necessary to uncover the overall circuit outcomes of DBS.

Low- and high-frequency STN-DBS exacerbates or improves motor function in parkinsonian animals, respectively, but does not alter movement in control animals [6, 51]. Therefore, elucidating the difference between control and parkinsonian mice in the modulation of the firing rate and the CV of the firing rate by low- and high-frequency stimulation may have implications for understanding the circuit bases of motor improvement by STN-DBS in parkinsonian animals. We found that, in parkinsonian mice, short-term and long-term electrical stimulation modulated the firing rate and the CV of the firing rate differently in STN−SNr and STN−GPi neurons. 6-OHDA lesion enhanced short-term electrical-stimulation-induced inhibition of type 1 STN−SNr neurons and short-term electrical-stimulation-induced excitation of STN−GPi neurons. This drastic contrast may be related to the reversal in the balance between excitatory and inhibitory synaptic inputs (from inhibition to excitation) observed in a considerable proportion of STN−GPi neurons in parkinsonian mice. In parkinsonian mice, 6-OHDA lesion enhanced the inhibition but attenuated the excitation induced by long-term electrical stimulation of STN−SNr and STN−GPi neurons. This may result in overall inhibition of STN neurons, which is an important reported outcome of STN DBS that improves motor outcomes [6, 47]. Long-term electrical stimulation increased the CV of the firing rate in STN neurons. A significant difference in this effect between control and parkinsonian mice was observed in STN−GPi neurons in response to long-term electrical stimulation at 20 and 50 Hz. Zhuang et al. demonstrated that regularization of the firing in STN neurons leads to improvement of motor deficits in parkinsonian rats [51]. In line with this, our data suggest that 20−50 Hz electrical stimulation may exacerbate irregularity in the firing of STN neurons in parkinsonian mice and result in deterioration of motor symptoms.

In addition to the SNr and GPi, the STN projects to other motor-related nuclei, including the globus pallidus externa, the substantia nigra pars compacta, the pedunculopontine nucleus, and the anterior thalamic nucleus, etc [1, 4, 15, 29, 39, 53–55]. Furthermore, these projection neurons may not be exclusively separable from each other [56–58]. Investigations combining more sophisticated retrograde tracing, molecule-specific labeling [59], and ex vivo and in vivo electrophysiological recordings (neuronal firing, synaptic inputs, and field potentials) are warranted to test the effects of DBS on individual STN projection neurons. Another limitation of the present study is that ex vivo brain slices preserve only the regional neural circuit, and electrical stimulation in brain slices recruits only a small sector of the global neural circuitry. In vivo studies demonstrate that high-frequency STN stimulation induces a reduction in firing rate and regularization of firing in STN neurons [4–7, 51]. We observed the former but not the latter. This inconsistency suggests that the global circuits, especially feedback loops that are absent from brain slices, may play an important role in determining the firing pattern in STN neurons. A further potential issue is that we isolated eIPSCs and eEPSCs biophysically. That is, we held the membrane potential of a neuron at the theoretical reversal potential of either Cl^- or cations to respectively record currents mediated by cation and Cl^- channels. With our K-gluconate-based intrapipette solution, the membrane potential

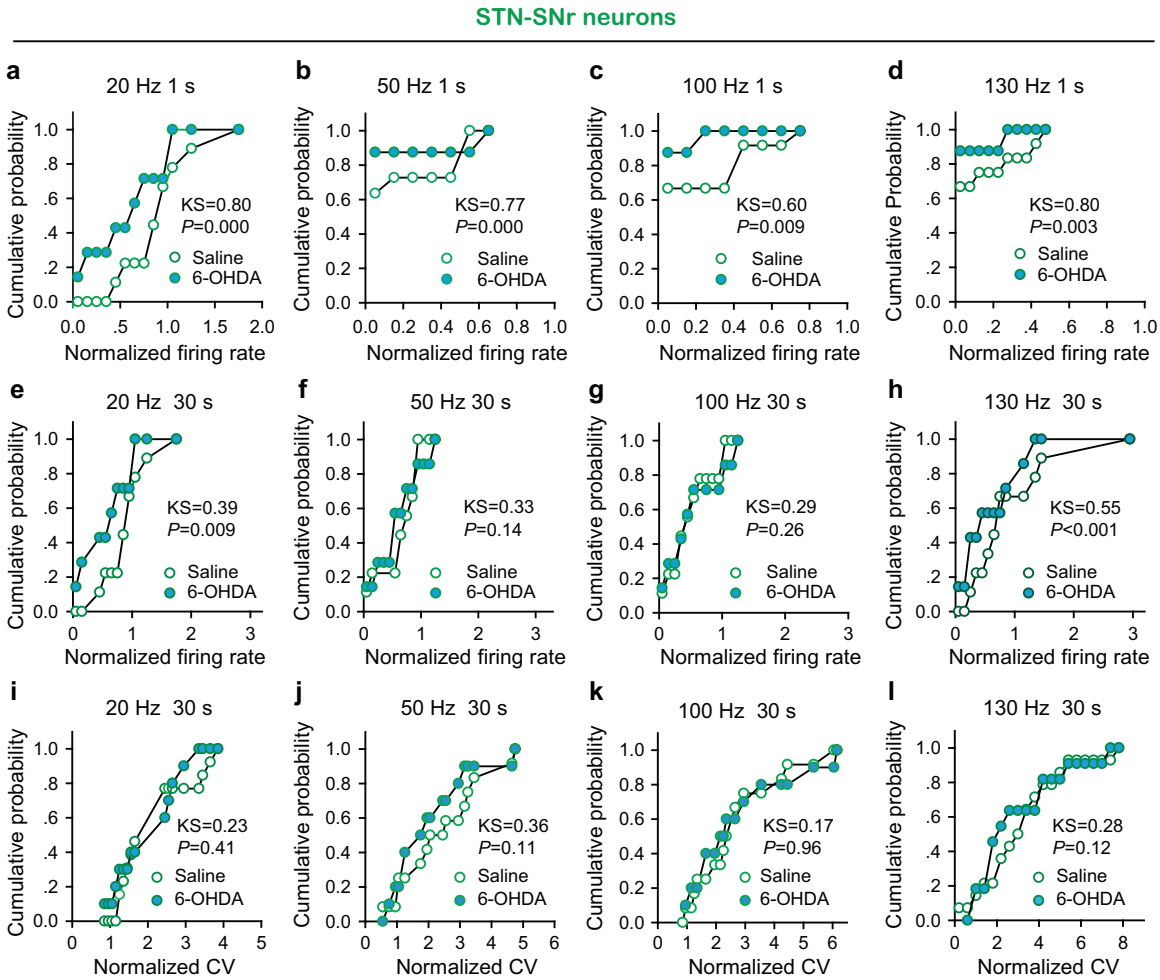

Fig. 5 Electrical stimulation of the STN modulates firing in STN−SNr neurons in control and parkinsonian mice. a–d Cumulative probability curves of the normalized firing rate during 1 s 20 Hz (**a**), 50 Hz (**b**), 100 Hz (**c**), and 130 Hz (**d**) electrical stimulation in type 1 STN −SNr neurons in Saline mice (open green circle, $n = 12$ from four mice) and 6-OHDA mice (solid green circle, $n = 8$ from four mice). **e–h** Cumulative probability curves of the normalized firing rate during 30 s 20 Hz (**e**), 50 Hz (**f**), 100 Hz (**g**), and 130 Hz (**h**) electrical stimulation in type 1 STN−SNr neurons in Saline mice (open green circle, $n = 12$ from four mice) and 6-OHDA mice (solid green circle, $n = 8$ from four mice). **i–l** Cumulative probability curves of the normalized CV of the firing rate during 1 s 20 Hz (**i**), 50 Hz (**j**), 100 Hz (**k**), and 130 Hz (**l**) electrical stimulation in type 1 STN−SNr neurons in Saline mice (open green circle, $n = 12$ from four mice) and 6-OHDA mice (solid green circle, $n = 8$ from three mice). The statistical significance of curve shifts was evaluated with K–S tests.

may not be controlled accurately at the intended holding potentials because potassium channels are persistently open at 0 mV. This caveat may affect the measurement of eIPSCs. However, we observed that the eIPSCs and eEPSCs in STN neurons were blocked by 10 μM GABAzine and 20 μM CNQX, respectively. This suggests that under our experimental conditions, the difference between the actual clamped voltage and the intended holding potential caused by the intrapipette solution may not have been so dramatic as to affect the receptor types mediating the eIPSCs and eEPSCs. Furthermore, although we may not have measured the eIPSCs accurately, the results we acquired from different groups of neurons remain eligible for comparison as the parameters were recorded under the same conditions. Finally, parkinsonian pathophysiology develops rapidly in the 6-OHDA-lesioned parkinsonian model and the resulting malfunctions in basal ganglia circuits may not be the same as in other parkinsonian models with slower disease progression. Further investigation is warranted to address whether the same properties and changes in STN−GPi neurons are also observed in neurotoxin-induced or genetically-modified slow-progressing parkinsonian animal models.

In conclusion, we have provided electrophysiological evidence showing that the predominance of inhibitory synaptic inputs was more apparent in STN−GPi neurons than in STN−SNr neurons; 6-OHDA lesion impaired the inhibitory inputs to STN−GPi neurons and reversed the input predominance from inhibitory to excitatory in these neurons; continuous electrical stimulation generally inhibited firing in both STN−SNr and STN−GPi neurons in parkinsonian mice, but low-frequency stimulation exacerbated firing irregularity in STN −GPi neurons in the parkinsonian condition. Therefore, STN−GPi neurons may be involved in both the pathophysiology of PD and DBS treatment of PD motor deficits.

ACKNOWLEDGEMENTS

This work was supported by the National Natural Science Foundation of China (81701100 (CYZ), 81870891 (CX), 81971038 (CYZ), 82071231 (CX), 82171235 (CYZ)), the Fund for Jiangsu Province Specially-Appointed Professor (CX, CYZ), the Natural Science Foundation of Jiangsu Province (BK20171160, BK20211349, CYZ), the Natural Science Foundation of the Jiangsu Higher Education Institutions of China (18KJA320009, CYZ), and the Start Fund from Xuzhou Medical University

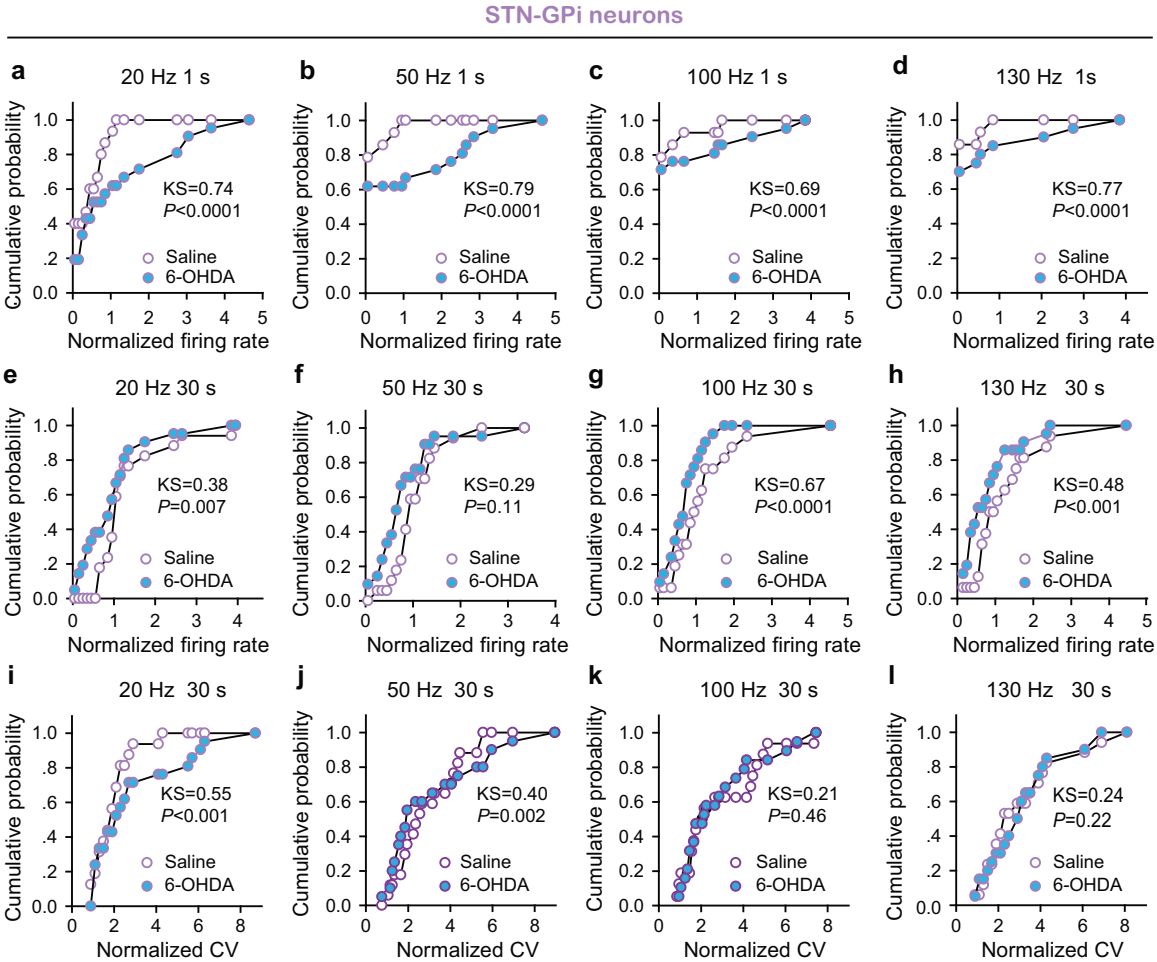

Fig. 6 Electrical stimulation of the STN modulates firing in STN−GPi neurons in control and parkinsonian mice. a–d Cumulative probability curves of the normalized firing rate during 1 s 20 Hz (**a**), 50 Hz (**b**), 100 Hz (**c**), and 130 Hz (**d**) electrical stimulation in STN−GPi neurons in Control mice (open purple circle, $n = 17$ from four mice) and 6-OHDA mice (purple circles filled with solid blue, $n = 21$ from four mice). **e–h** Cumulative probability curves of the normalized firing rate during 30 s 20 Hz (**e**), 50 Hz (**f**), 100 Hz (**g**), and 130 Hz (**h**) electrical stimulation in STN−GPi neurons in Control mice (open purple circle, $n = 17$ from four mice) and 6-OHDA mice (purple circle filled with solid blue, $n = 21$ from four mice). **i–l** Cumulative probability curves of the normalized CV of the firing rate during 30 s 20 Hz (**i**), 50 Hz (**j**), 100 Hz (**k**), and 130 Hz (**l**) electrical stimulation in type 1 STN−GPi neurons in Control mice (open green circle $n = 12$ from four mice) and 6-OHDA mice (purple circle filled with solid blue, $n = 8$ from three mice). The statistical significance of curve shifts was evaluated with K–S tests.

(D2017009, D2017010). YWJ and TJ acknowledge the Postgraduate Innovation Program in Jiangsu Province (KYCX20_2474, KYCX20_2478).

AUTHOR CONTRIBUTIONS

CX and CYZ designed and supervised this research. CX and CYZ collected, analyzed and illustrated the electrophysiological data. YWJ, YWL, and TJ performed the mouse survival surgeries and histological experiments. YJ and TJ performed the behavioral tests. YWJ, YWL, and CY managed the mouse colony. CX and CYZ collected the imaging data. CX and CYZ wrote the paper. All authors read and approved the paper.

ADDITIONAL INFORMATION

Competing interests: The authors declare no competing interests.

REFERENCES

1. Benarroch EE. Subthalamic nucleus and its connections: anatomic substrate for the network effects of deep brain stimulation. Neurology. 2008;70:1991–5.
2. Bonnevie T, Zaghloul KA. The subthalamic nucleus: unravelling new roles and mechanisms in the control of action. Neuroscientist. 2019;25:48–64.
3. Fife KH, Gutierrez-Reed NA, Zell V, Bailly J, Lewis CM, Aron AR, et al. Causal role for the subthalamic nucleus in interrupting behavior. Elife. 2017;6:e27689.
4. Hamani C, G. F, Heinsen H, Plantinga BR, Temel Y, Uludag K, et al. Subthalamic nucleus deep brain stimulation: Basic concepts and novel perspectives. eNeuro. 2017;4:0140–17.
5. Faggiani E, Benazzouz A. Deep brain stimulation of the subthalamic nucleus in Parkinson's disease: from history to the interaction with the monoaminergic systems. Prog Neurobiol. 2017;151:139–56.
6. Gradinaru V, Mogri M, Thompson KR, Henderson JM, Deisseroth K. Optical deconstruction of parkinsonian neural circuitry. Science. 2009;324:354–9.
7. Sanders TH, Jaeger D. Optogenetic stimulation of cortico-subthalamic projections is sufficient to ameliorate bradykinesia in 6-ohda lesioned mice. Neurobiol Dis. 2016;95:225–37.
8. Yoon HH, Park JH, Kim YH, Min J, Hwang E, Lee CJ, et al. Optogenetic inactivation of the subthalamic nucleus improves forelimb akinesia in a rat model of Parkinson disease. Neurosurgery. 2014;74:533–40. discussion 40-41
9. Chu HY, Atherton JF, Wokosin D, Surmeier DJ, Bevan MD. Heterosynaptic regulation of external globus pallidus inputs to the subthalamic nucleus by the motor cortex. Neuron. 2015;85:364–76.
10. Chu HY, McIver EL, Kovaleski RF, Atherton JF, Bevan MD. Loss of hyperdirect pathway cortico-subthalamic inputs following degeneration of midbrain dopamine neurons. Neuron. 2017;95:1306–18.
11. Wang YY, Wang Y, Jiang HF, Liu JH, Jia J, Wang K, et al. Impaired glutamatergic projection from the motor cortex to the subthalamic nucleus in 6-hydroxydopamine-lesioned hemi-parkinsonian rats. Exp Neurol. 2018;300:135–48.

12. Mazzone P, Scarnati E, Garcia-Rill E. Commentary: the pedunculopontine nucleus: clinical experience, basic questions and future directions. J Neural Transm (Vienna). 2011;118:1391–6.
13. Yu C, Cassar IR, Sambangi J, Grill WM. Frequency-specific optogenetic deep brain stimulation of subthalamic nucleus improves Parkinsonian motor behaviors. J Neurosci. 2020;40:4323–34.
14. Lin JY. A user's guide to channelrhodopsin variants: features, limitations and future developments. Exp Physiol. 2011;96:19–25.
15. Marani E, Heida T, Lakke EA, Usunoff KG. The subthalamic nucleus. Part I: Development, cytology, topography and connections. Adv Anat Embryol Cell Biol. 2008;198:1–113. vii
16. Heida T, Marani E, Usunoff KG. The subthalamic nucleus part II: modelling and simulation of activity. Adv Anat Embryol Cell Biol. 2008;199:1–85. vii
17. Windels F, Bruet N, Poupard A, Feuerstein C, Bertrand A, Savasta M. Influence of the frequency parameter on extracellular glutamate and gamma-aminobutyric acid in substantia nigra and globus pallidus during electrical stimulation of subthalamic nucleus in rats. J Neurosci Res. 2003;72:259–67.
18. Zhang B, Chu J, Zhang J, Ma Y. Change of extracellular glutamate and gamma-aminobutyric acid in substantia nigra and globus pallidus during electrical stimulation of subthalamic nucleus in epileptic rats. Stereotact Funct Neurosurg. 2008;86:208–15.
19. Guridi J, Rodriguez-Rojas R, Carmona-Abellan M, Parras O, Becerra V, Lanciego JL. History and future challenges of the subthalamic nucleus as surgical target: Review article. Mov Disord. 2018;33:1540–50.
20. Odekerken VJ, Boel JA, Schmand BA, de Haan RJ, Figee M, van den Munckhof P, et al. GPi vs STN deep brain stimulation for Parkinson disease: Three-year follow-up. Neurology. 2016;86:755–61.
21. Ramirez-Zamora A, Ostrem JL. Globus pallidus interna or subthalamic nucleus deep brain stimulation for Parkinson disease: a review. JAMA Neurol. 2018;75:367–72.
22. Valldeoriola F, Munoz E, Rumia J, Roldan P, Camara A, Compta Y, et al. Simultaneous low-frequency deep brain stimulation of the substantia nigra pars reticulata and high-frequency stimulation of the subthalamic nucleus to treat levodopa unresponsive freezing of gait in Parkinson's disease: a pilot study. Parkinsonism Relat Disord. 2019;60:153–7.
23. Collomb-Clerc A, Welter ML. Effects of deep brain stimulation on balance and gait in patients with Parkinson's disease: a systematic neurophysiological review. Neurophysiol Clin. 2015;45:371–88.
24. Heilbronn M, Scholten M, Schlenstedt C, Mancini M, Schollmann A, Cebi I, et al. Anticipatory postural adjustments are modulated by substantia nigra stimulation in people with Parkinson's disease and freezing of gait. Parkinsonism Relat Disord. 2019;66:34–9.
25. Assaf F, Schiller Y. A chemogenetic approach for treating experimental Parkinson's disease. Mov Disord. 2019;34:469–79.
26. Sobesky L, Goede L, Odekerken VJJ, Wang Q, Li N, Neudorfer C, et al. Subthalamic and pallidal deep brain stimulation: are we modulating the same network? Brain. 2021. https://doi.org/10.1093/brain/awab258.
27. Zhang C, Lai Y, Li J, He N, Liu Y, Li Y, et al. Subthalamic and pallidal stimulations in patients with Parkinson's disease: common and dissociable connections. Ann Neurol. 2021. https://doi.org/10.1002/ana.26199.
28. Tervo DG, Hwang BY, Viswanathan S, Gaj T, Lavzin M, Ritola KD, et al. A designer AAV variant permits efficient retrograde access to projection neurons. Neuron. 2016;92:372–82.
29. Xiao C, Cho JR, Zhou C, Treweek JB, Chan K, McKinney SL, et al. Cholinergic mesopontine signals govern locomotion and reward through dissociable midbrain pathways. Neuron. 2016;90:333–47.
30. Xiao C, Miwa JM, Henderson BJ, Wang Y, Deshpande P, McKinney SL, et al. Nicotinic receptor subtype-selective circuit patterns in the subthalamic nucleus. J Neurosci. 2015;35:3734–46.
31. Luan Y, Tang D, Wu H, Gu W, Wu Y, Cao JL, et al. Reversal of hyperactive subthalamic circuits differentially mitigates pain hypersensitivity phenotypes in parkinsonian mice. Proc Natl Acad Sci USA. 2020;117:10045–54.
32. Zhou C, Gu W, Wu H, Yan X, Deshpande P, Xiao C, et al. Bidirectional dopamine modulation of excitatory and inhibitory synaptic inputs to subthalamic neuron subsets containing alpha4beta2 or alpha7 nAChRs. Neuropharmacology. 2019;148:220–8.
33. Cenci MA, Lundblad M. Ratings of L-DOPA-induced dyskinesia in the unilateral 6-OHDA lesion model of Parkinson's disease in rats and mice. Curr Protoc Neurosci. 2007; Chapter 9: Unit 9 25. 1–23.
34. Noldus LP, Spink AJ, Tegelenbosch RA. EthoVision: a versatile video tracking system for automation of behavioral experiments. Behav Res Methods Instrum Comput. 2001;33:398–414.
35. Blandini F, Armentero MT, Martignoni E. The 6-hydroxydopamine model: news from the past. Parkinsonism Relat Disord. 2008;14:S124–9. Suppl 2
36. Schneider CA, Rasband WS, Eliceiri KW. NIH Image to ImageJ: 25 years of image analysis. Nat Methods. 2012;9:671.
37. Benabid AL, Chabardes S, Mitrofanis J, Pollak P. Deep brain stimulation of the subthalamic nucleus for the treatment of Parkinson's disease. Lancet Neurol. 2009;8:67–81.
38. Schor JS, Nelson AB. Multiple stimulation parameters influence efficacy of deep brain stimulation in parkinsonian mice. J Clin Invest. 2019;130:3833–8.
39. Steiner LA, Barreda Tomas FJ, Planert H, Alle H, Vida I, Geiger JRP. Connectivity and dynamics underlying synaptic control of the subthalamic nucleus. J Neurosci. 2019;39:2470–81.
40. Wilson CL, Puntis M, Lacey MG. Overwhelmingly asynchronous firing of rat subthalamic nucleus neurones in brain slices provides little evidence for intrinsic interconnectivity. Neuroscience. 2004;123:187–200.
41. Atherton JF, Kitano K, Baufreton J, Fan K, Wokosin D, Tkatch T, et al. Selective participation of somatodendritic HCN channels in inhibitory but not excitatory synaptic integration in neurons of the subthalamic nucleus. J Neurosci. 2010;30:16025–40.
42. Bevan MD, Hallworth NE, Baufreton J. GABAergic control of the subthalamic nucleus. Prog Brain Res. 2007;160:173–88.
43. Wang L, Kitai ST, Xiang Z. Activity-dependent bidirectional modification of inhibitory synaptic transmission in rat subthalamic neurons. J Neurosci. 2006;26:7321–7.
44. Akram H, Sotiropoulos SN, Jbabdi S, Georgiev D, Mahlknecht P, Hyam J, et al. Subthalamic deep brain stimulation sweet spots and hyperdirect cortical connectivity in Parkinson's disease. Neuroimage. 2017;158:332–45.
45. Parent A, Hazrati LN. Functional anatomy of the basal ganglia. II. The place of subthalamic nucleus and external pallidum in basal ganglia circuitry. Brain Res Brain Res Rev. 1995;20:128–54.
46. Rinvik E, Ottersen OP. Terminals of subthalamonigral fibres are enriched with glutamate-like immunoreactivity: an electron microscopic, immunogold analysis in the cat. J Chem Neuroanat. 1993;6:19–30.
47. Milosevic L, Kalia SK, Hodaie M, Lozano AM, Fasano A, Popovic MR, et al. Neuronal inhibition and synaptic plasticity of basal ganglia neurons in Parkinson's disease. Brain. 2018;141:177–90.
48. Hallworth NE, Bevan MD. Globus pallidus neurons dynamically regulate the activity pattern of subthalamic nucleus neurons through the frequency-dependent activation of postsynaptic GABAA and GABAB receptors. J Neurosci. 2005;25:6304–15.
49. Kita H, Chiken S, Tachibana Y, Nambu A. Origins of GABA(A) and GABA(B) receptor-mediated responses of globus pallidus induced after stimulation of the putamen in the monkey. J Neurosci. 2006;26:6554–62.
50. McIver EL, Atherton JF, Chu HY, Cosgrove KE, Kondapalli J, Wokosin D, et al. Maladaptive downregulation of autonomous subthalamic nucleus activity following the loss of midbrain dopamine neurons. Cell Rep. 2019;28:992–1002 e4.
51. Zhuang QX, Li GY, Li B, Zhang CZ, Zhang XY, Xi K, et al. Regularizing firing patterns of rat subthalamic neurons ameliorates parkinsonian motor deficits. J Clin Invest. 2018;128:5413–27.
52. Baufreton J, Bevan MD. D2-like dopamine receptor-mediated modulation of activity-dependent plasticity at GABAergic synapses in the subthalamic nucleus. J Physiol. 2008;586:2121–42.
53. Alkemade A, Schnitzler A, Forstmann BU. Topographic organization of the human and non-human primate subthalamic nucleus. Brain Struct Funct. 2015;220:3075–86.
54. Barter JW, Castro S, Sukharnikova T, Rossi MA, Yin HH. The role of the substantia nigra in posture control. Eur J Neurosci. 2014;39:1465–73.
55. Zhang H, Zhang CK, Qu ZW, Li B, Su YJ, Li X, et al. STN-ANT plasticity is crucial for the motor control in Parkinson's disease model. Signal Transduct Target Ther. 2021;6. https://doi.org/10.1038/s41392-021-00545-z.
56. Koshimizu Y, Fujiyama F, Nakamura KC, Furuta T, Kaneko T. Quantitative analysis of axon bouton distribution of subthalamic nucleus neurons in the rat by single neuron visualization with a viral vector. J Comp Neurol. 2013;521:2125–46.
57. Sato F, Parent M, Levesque M, Parent A. Axonal branching pattern of neurons of the subthalamic nucleus in primates. J Comp Neurol. 2000;424:142–52.
58. Van Der Kooy D, Hattori T. Single subthalamic nucleus neurons project to both the globus pallidus and substantia nigra in rat. J Comp Neurol. 1980;192:751–68.
59. Parolari L, Schneeberger M, Heintz N, Friedman JM. Functional analysis of distinct populations of subthalamic nucleus neurons on Parkinson's disease and OCD-like behaviors in mice. Mol Psychiatry. 2021. https://doi.org/10.1038/s41380-021-01162-6.